

REPORT DOCUMENTATION PAGE			Form Approved OMB NO. 0704-0188		
<p>The public reporting burden for this collection of information is estimated to average 1 hour per response, including the time for reviewing instructions, searching existing data sources, gathering and maintaining the data needed, and completing and reviewing the collection of information. Send comments regarding this burden estimate or any other aspect of this collection of information, including suggestions for reducing this burden, to Washington Headquarters Services, Directorate for Information Operations and Reports, 1215 Jefferson Davis Highway, Suite 1204, Arlington VA, 22202-4302. Respondents should be aware that notwithstanding any other provision of law, no person shall be subject to any penalty for failing to comply with a collection of information if it does not display a currently valid OMB control number. PLEASE DO NOT RETURN YOUR FORM TO THE ABOVE ADDRESS.</p>					
1. REPORT DATE (DD-MM-YYYY) 03-11-2018		2. REPORT TYPE Final Report		3. DATES COVERED (From - To) 16-Aug-2010 - 15-Aug-2017	
4. TITLE AND SUBTITLE Final Report: High-Resolution DoA Determination with Electrically Small Antenna Arrays			5a. CONTRACT NUMBER W911NF-10-1-0274		
			5b. GRANT NUMBER		
			5c. PROGRAM ELEMENT NUMBER 611102		
6. AUTHORS			5d. PROJECT NUMBER		
			5e. TASK NUMBER		
			5f. WORK UNIT NUMBER		
7. PERFORMING ORGANIZATION NAMES AND ADDRESSES University of Illinois - Urbana - Champaign c/o Office of Sponsored Programs 1901 S. First Street, Suite A Champaign, IL 61820 -7406			8. PERFORMING ORGANIZATION REPORT NUMBER		
9. SPONSORING/MONITORING AGENCY NAME(S) AND ADDRESS (ES) U.S. Army Research Office P.O. Box 12211 Research Triangle Park, NC 27709-2211			10. SPONSOR/MONITOR'S ACRONYM(S) ARO		
			11. SPONSOR/MONITOR'S REPORT NUMBER(S) 56985-EL.11		
12. DISTRIBUTION AVAILABILITY STATEMENT Approved for public release; distribution is unlimited.					
13. SUPPLEMENTARY NOTES The views, opinions and/or findings contained in this report are those of the author(s) and should not be construed as an official Department of the Army position, policy or decision, unless so designated by other documentation.					
14. ABSTRACT					
15. SUBJECT TERMS					
16. SECURITY CLASSIFICATION OF:		17. LIMITATION OF ABSTRACT	15. NUMBER OF PAGES	19a. NAME OF RESPONSIBLE PERSON	
a. REPORT	b. ABSTRACT			c. THIS PAGE	Jennifer Bernhard
UU	UU	UU	UU	19b. TELEPHONE NUMBER 217-333-3029	

RPPR Final Report
as of 05-Nov-2018

Agency Code:

Proposal Number: 56985EL

Agreement Number: W911NF-10-1-0274

INVESTIGATOR(S):

Name: Douglas L. Jones
Email: DL-Jones@uiuc.edu
Phone Number: 2172446823
Principal: N

Name: Jennifer Bernhard
Email: jbernar@illinois.edu
Phone Number: 21733330293
Principal: Y

Organization: **University of Illinois - Urbana - Champaign**

Address: c/o Office of Sponsored Programs, Champaign, IL 618207406

Country: USA

DUNS Number: 041544081

EIN: 376000511

Report Date: 15-Nov-2017

Date Received: 03-Nov-2018

Final Report for Period Beginning 16-Aug-2010 and Ending 15-Aug-2017

Title: High-Resolution DoA Determination with Electrically Small Antenna Arrays

Begin Performance Period: 16-Aug-2010

End Performance Period: 15-Aug-2017

Report Term: 0-Other

Submitted By: Jennifer Bernhard

Email: jbernar@illinois.edu

Phone: (217) 333-30293

Distribution Statement: 1-Approved for public release; distribution is unlimited.

STEM Degrees: 0

STEM Participants: 1

Major Goals: The major goal of the extension of this project is the investigation of broadband design techniques for microstrip antenna arrays, as specified by the sponsor, LPS.

Accomplishments: Please see the uploaded report file.

Training Opportunities: The project supported one graduate student, Ayah Massoud, to perform this research as part of her graduate training.

Results Dissemination: The following related conference paper was presented earlier in the program period and formed the basis of the present work.

A. T. Massoud and J. T. Bernhard, "A dual-band dual-polarized steerable pattern reconfigurable antenna," in Proc. 2015 IEEE/URSI International Symposium on Antennas and Propagation, Vancouver, Canada, July 2015, pp. 2235-2236.

The antennas used in the subsequent work were inspired by what we learned in this initial research.

Honors and Awards: Nothing to Report

Protocol Activity Status:

Technology Transfer: Nothing to Report

PARTICIPANTS:

Participant Type: PD/PI

Participant: Jennifer Truman Bernhard

RPPR Final Report
as of 05-Nov-2018

Person Months Worked: 1.00

Funding Support:

Project Contribution:
International Collaboration:
International Travel:
National Academy Member: N
Other Collaborators:

Participant Type: Graduate Student (research assistant)

Participant: Ayah Massoud

Person Months Worked: 8.00

Funding Support:

Project Contribution:
International Collaboration:
International Travel:
National Academy Member: N
Other Collaborators:

ARTICLES:

Publication Type: Journal Article

Peer Reviewed: Y

Publication Status: 1-Published

Journal: IEEE Transactions on Antennas and Propagation

Publication Identifier Type: DOI

Publication Identifier: 10.1109/TAP.2012.2227921

Volume: 61

Issue: 3

First Page #: 0

Date Submitted:

Date Published:

Publication Location:

Article Title: Demonstration of an Electrically Small Antenna Array for UHF Direction-of-Arrival Estimation

Authors:

Keywords: Direction-of-arrival (DoA), electrically small antenna,multiple signal classification (MuSiC), minimum-variancedistortionless response (MVDR), vector sensor

Abstract: Direction-of-arrival (DoA) estimation of incoming electromagnetic signals can play a critical role in surveillance, sensing, and cognitive radio applications. Typical DoA antenna arrays use an aperture measuring several wavelengths across to ensure reliable measurement of phase information. For a UHF application, such an array would need to be a few meters across—too large for a portable array. This work demonstrates a practical DoA array composed of antennas with diverse radiation patterns which is combined with an algorithm which relies primarily on amplitude information rather than phase information. This approach yields a much smaller array with similar direction-finding capabilities to larger ones. A calibration procedure captures the antenna responses, including the parasitic effects of the closely spaced antennas. The calibrated array and direction-finding algorithm then achieves measured accuracy with resolution of six degrees with no front-to-back or quadrant ambiguities.

Distribution Statement: 1-Approved for public release; distribution is unlimited.

Acknowledged Federal Support:

CONFERENCE PAPERS:

Publication Type: Conference Paper or Presentation

Publication Status: 1-Published

Conference Name: Antenna Applications Symposium

Date Received: 07-Jul-2016

Conference Date: 21-Sep-2011

Date Published: 21-Sep-2011

Conference Location: Monticello, IL

Paper Title: Resolution limitations in UHF direction of arrival estimation using electrically small arrays

Authors: Matthew Slater, Christopher Schmitz, Douglas Jones, Jennifer Bernhard

Acknowledged Federal Support: Y

RPPR Final Report
as of 05-Nov-2018

DISSERTATIONS:

Publication Type: Thesis or Dissertation

Institution:

Date Received: 24-Jan-2013

Completion Date:

Title: DESIGN AND ANALYSIS OF DIRECTION-OF-ARRIVAL ESTIMATION SYSTEMS USING ELECTRICALLY SMALL ANTENNA ARRAYS

Authors:

Acknowledged Federal Support:

Publication Type: Thesis or Dissertation

Institution:

Date Received: 15-Apr-2015

Completion Date:

Title: AN ELECTRICALLY SMALL MULTI-PORT LOOP ANTENNA FOR DIRECTION OF ARRIVAL ESTIMATION

Authors:

Acknowledged Federal Support:

Publication Type: Thesis or Dissertation

Institution: University of Illinois at Urbana-Champaign

Date Received: 07-Jul-2016

Completion Date: 5/16/09 12:04AM

Title: An Investigation into Electrically Small Antennas Used for Direction of Arrival Estimation

Authors: Michael Anderson

Acknowledged Federal Support: **Y**

Publication Type: Thesis or Dissertation

Institution: University of Illinois at Urbana-Champaign

Date Received: 07-Jul-2016

Completion Date: 12/16/14 3:49AM

Title: An Investigation of Series LC Resonant Circuits with a Sleeve Balun to Achieve Wideband Operation

Authors: Christie Bermudez Rivera

Acknowledged Federal Support: **Y**

Publication Type: Thesis or Dissertation

Institution: University of Illinois at Urbana-Champaign

Date Received: 03-Nov-2018

Completion Date: 4/29/16 8:44PM

Title: MEASUREMENT OF ANTENNA RADIATION EFFICIENCY USING IMPROVED WHEELER CAP ALGORITHM

Authors: Elias Wilken-Resman

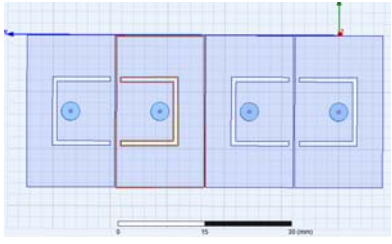
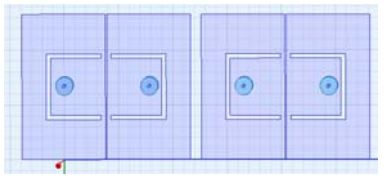
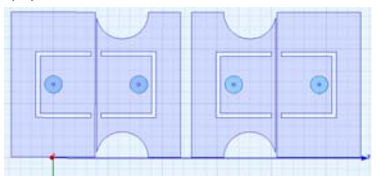
Acknowledged Federal Support: **Y**

**A Small Linear Ultra-wideband Microstrip Antenna Array:
Further Bandwidth Enhancement, Reduction of Coupled Energies and Improvement of Bandwidth
Symmetry between Inner and Outer Elements**

A. Massoud and J. T. Bernhard
Electromagnetics Laboratory, Department of Electrical and Computer Engineering
University of Illinois at Urbana-Champaign

Introduction

The previous year's design's strategy was to improve the bandwidth of the four-element array by introducing semi-circular cutouts in the center elements. This improved the inner element performance but at the expense of the outer element's bandwidth, causing a measurable asymmetry. Table 1 summarizes the evolution of the design process and the bandwidth performance. Each consecutive design arises to mitigate a problem or improve upon the predecessor. The benefit of each design and the motivation behind each variation is discussed in the next section. The first three designs were previously discussed and analyzed. Designs (4), (5) and (6) are new for this performance period and will be discussed in detail.

Design	Outer Element			Inner Element			Relative BW (outer element : inner element)
	f_{min} GHz	f_{max} GHz	BW (GHz) (%)	f_{min} GHz	f_{max} GHz	BW (GHz) (%)	
(1) 	3.59	5.27	1.68 (1.47:1) (37.9%)	3.57	5.80	2.23 (1.62:1) (47.6%)	0.75
(2) 	3.53	5.84	2.31 (1.65:1) (49.3%)	3.54	6.00	2.46 (1.69:1) (51.6%)	0.93
(3) 	3.62	5.51	1.99 (1.52:1) (43.1%)	3.13	6.03	2.90 (1.93:1) (63.3%)	0.69

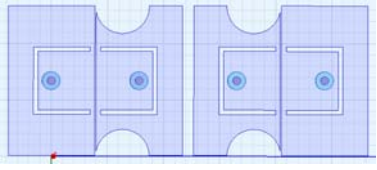
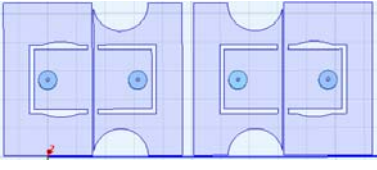
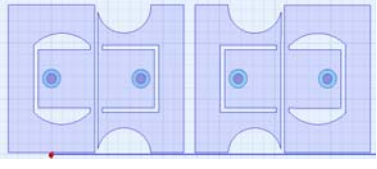
(4)		4.49	7.23	2.74 (1.61:1) (46.8%)	4.30	7.89	3.59 (1.83:1) (58.9%)	0.76
(5)		3.51	5.90	2.39 (1.68:1) (50.8%)	3.16	6.01	2.85 (1.90:1) (62.2%)	0.84
(6)		3.46	7.04	3.58 (2.16:1) (68.2%)	3.54	7.91	4.37 (2.23:1) (76.3%)	0.82

Table 1: A summary of each design showing the geometry, lower and upper frequency limits of the bandwidth and the dynamic range for the inner and outer elements.

Design evolution

Design (1): Simply arraying four U-slot antennas symmetrically resulted in improved bandwidth for the center element. However, the bandwidth is lower for the edge element compared to the two element case causing bandwidth asymmetry that Design (2) mitigates.

Design (2): Separating each pair of the four-element array increased the bandwidth for both center and edge elements and improved the symmetry.

Design (3): This design attempts to improve the bandwidth further by introducing semi-circular cutouts in the center elements. This improvement is due to a lowering of the lower frequency limit in the center element's bandwidth and hence an increased current path on the patch. However, this improvement was not transferred to the edge element increasing the asymmetry again. A second issue is the high coupled energy in the 4 GHz frequency range.

Designs (4) and (5) attempt to solve these two issues separately while Design (6) combines (4) and (5) for an overall improvement.

Design (4): Increasing Probe Radius

It is initially hypothesized that increasing the radius of the probe feeding the patches will shift the frequency response to the right, i.e. increasing both the lower and upper frequency limits of the bandwidth. The reason is that the capacitance of a cylindrical conductor varies as $1/\log(b/a)$, where a is the inner conductor's radius, so a larger radius increases the capacitance and increases higher frequency admittance. Keeping all other parameters constant, the radius in Design (3) was increased and simulated for each case from 0.3 mm to 1 mm.

Figures 1 and 2 show the bandwidth behavior for center and edge elements at different radii. As the radius is increased, the $VSWR < 2$ range shifts to the right. The red trace (0.3 mm) case has a low VSWR for 3 GHz range and a high VSWR for 7 GHz range and vice versa for the orange trace (1 mm).

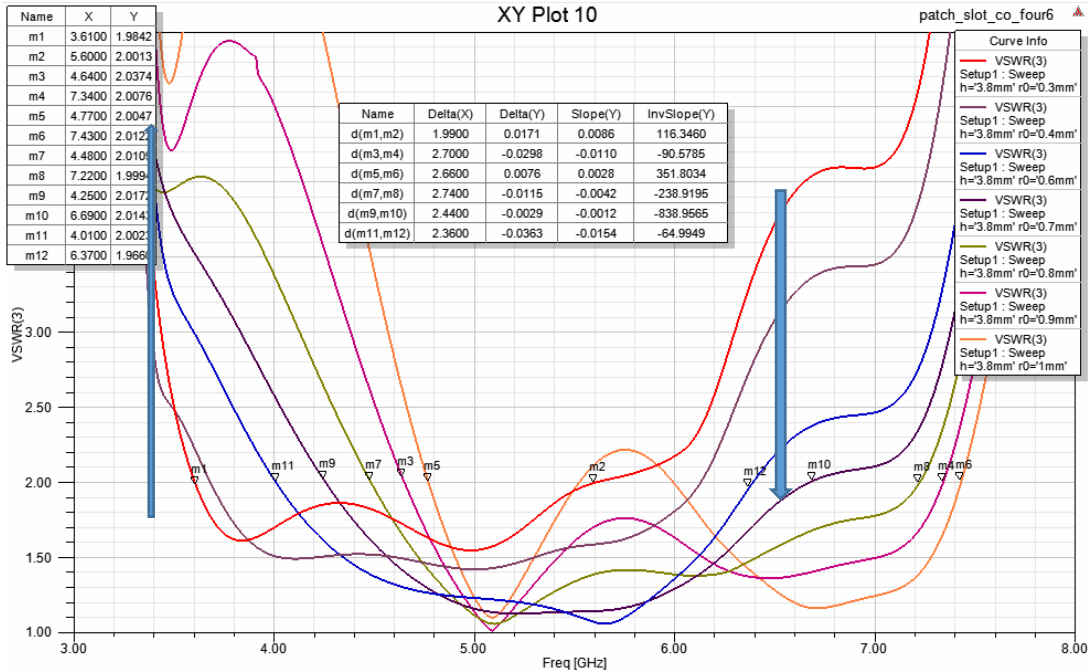


Figure 1: Bandwidth behavior for inner element for different radii. The arrows indicate the general trend when increasing the probe radius.

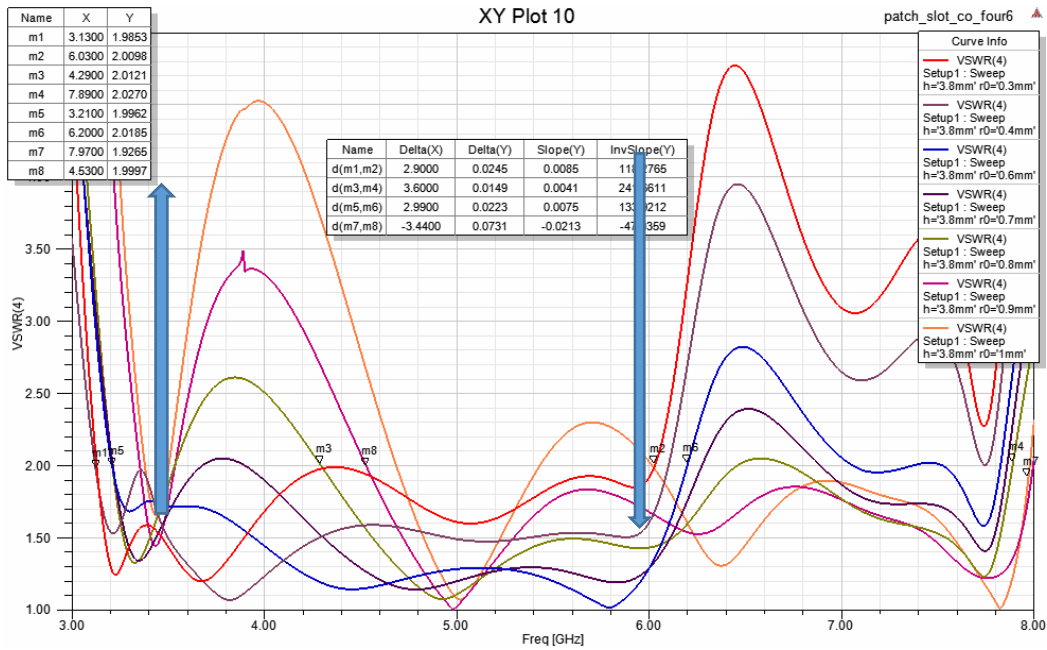


Figure 2: bandwidth behavior for outer element for different radii. The arrows indicate the general trend when increasing the probe radius.

In both figures, the 0.8 mm trace has the largest bandwidth. The reasoning explained above is verified by observing the Smith chart of the input impedance. Figures 3 and 4 show the response has shifted downwards towards the center line indicating a lower reactance due to an increase in capacitance.

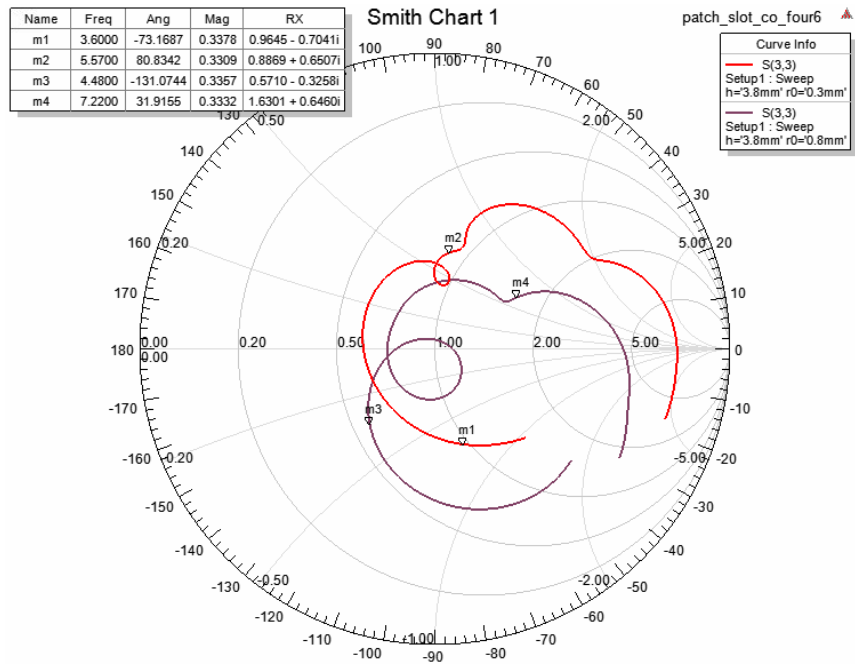


Figure 3: Smith chart for inner element. The red trace is the 0.3 mm and purple trace is the 0.8 mm.

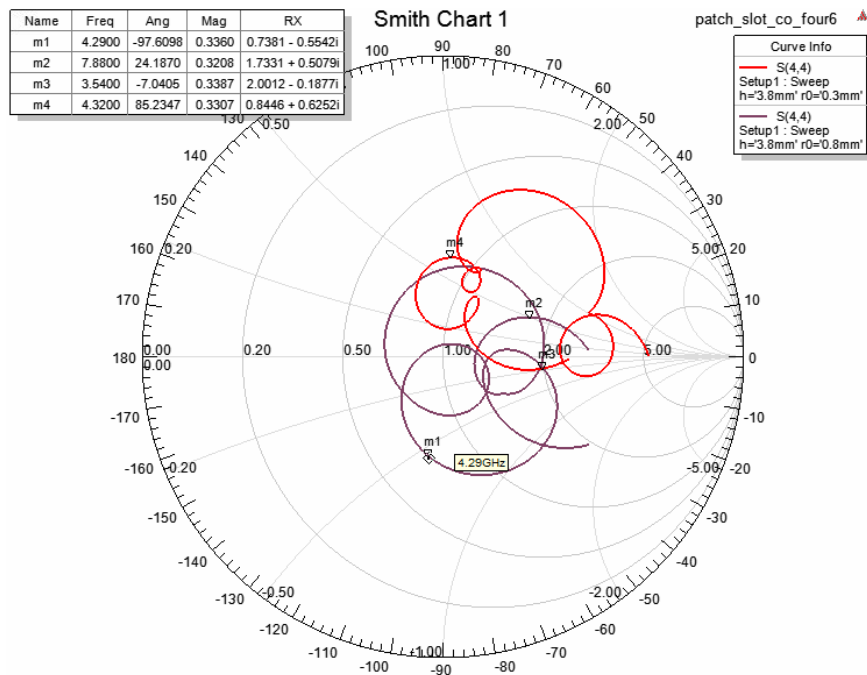


Figure 4: Smith chart for the outer element. The red trace is the 0.3 mm and the purple trace is the 0.8 mm case.

Figures 5 and 6 show the input impedance plots for the inner and outer elements. As a consequence of the lower reactance, the design has more resonance points in the frequency range as observed in the blue dashed versus the red dashed traces crossing the horizontal axis.

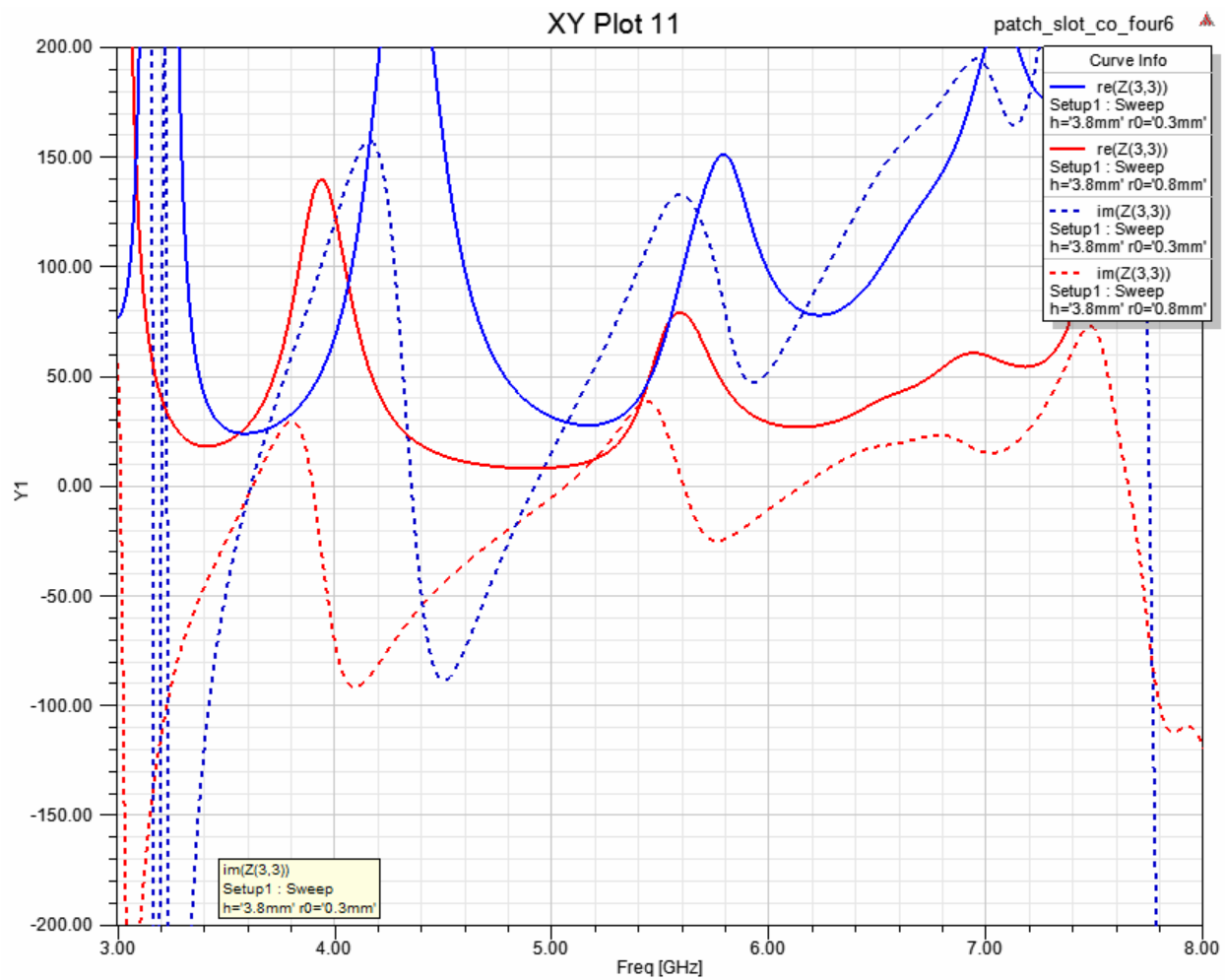


Figure 5: Input impedance of the outer element for the 0.3 mm case (blue trace) and 0.8 mm case (red trace). Solid traces are the real part of the impedance. Dashed traces are the imaginary part of the impedance.

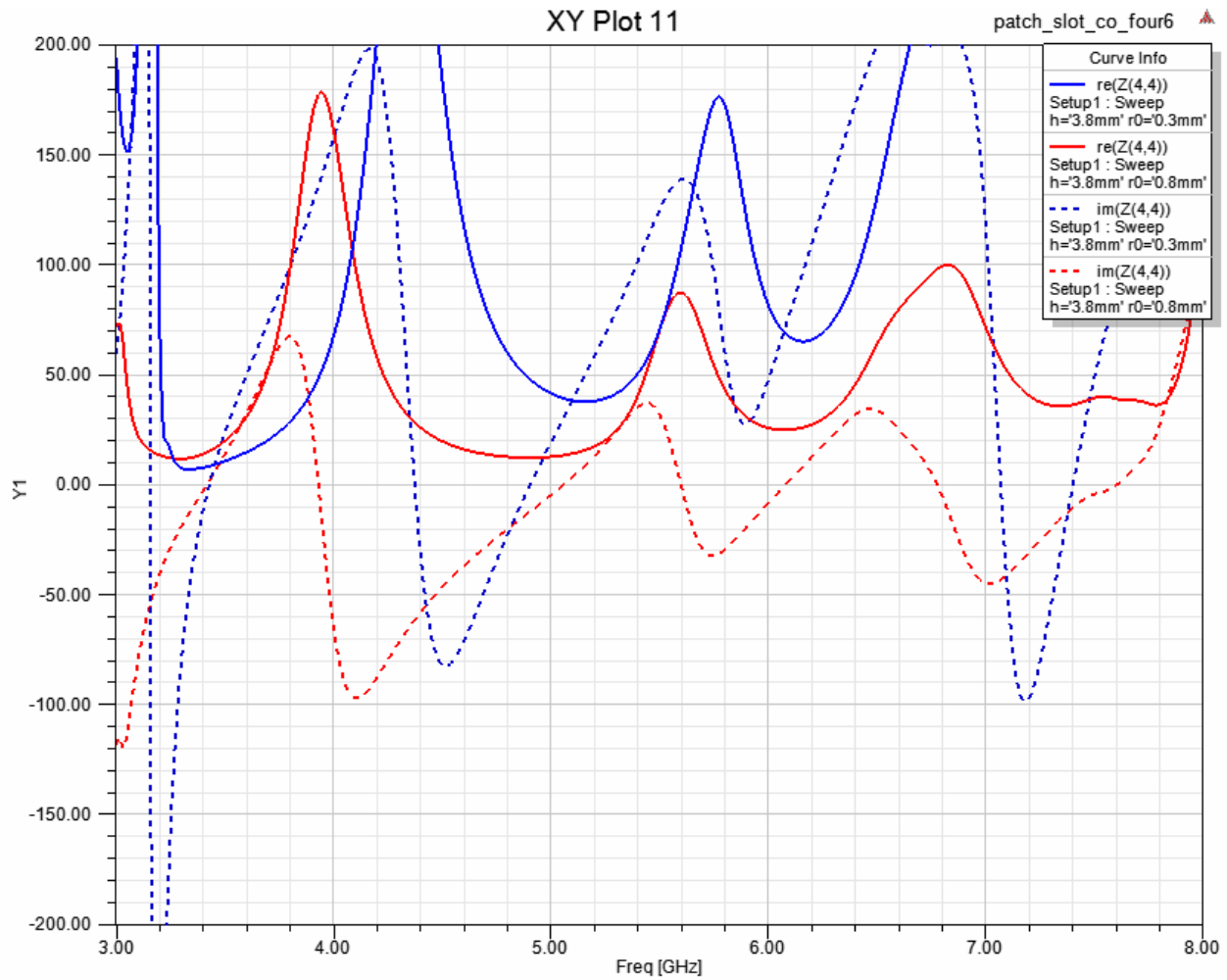
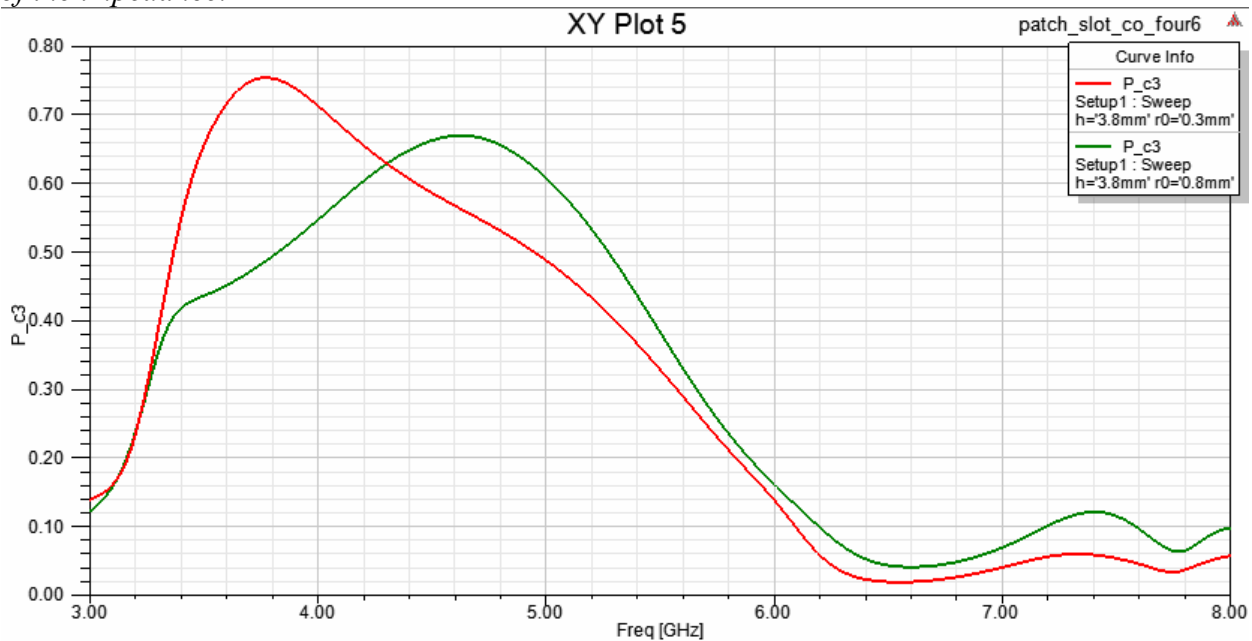
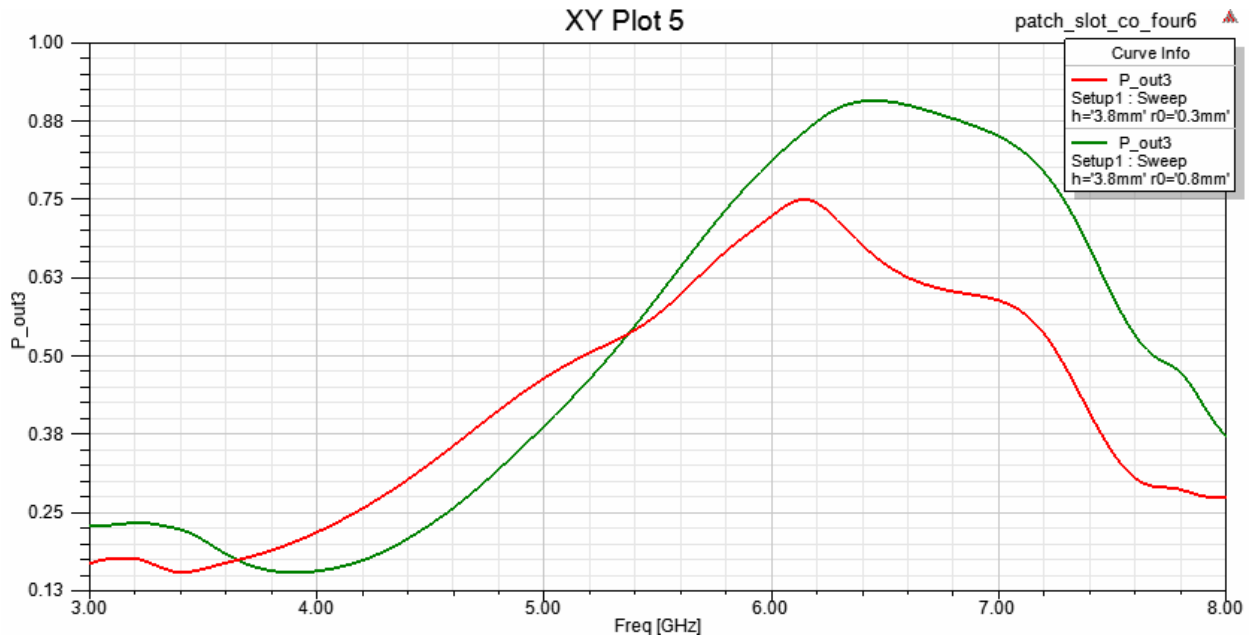


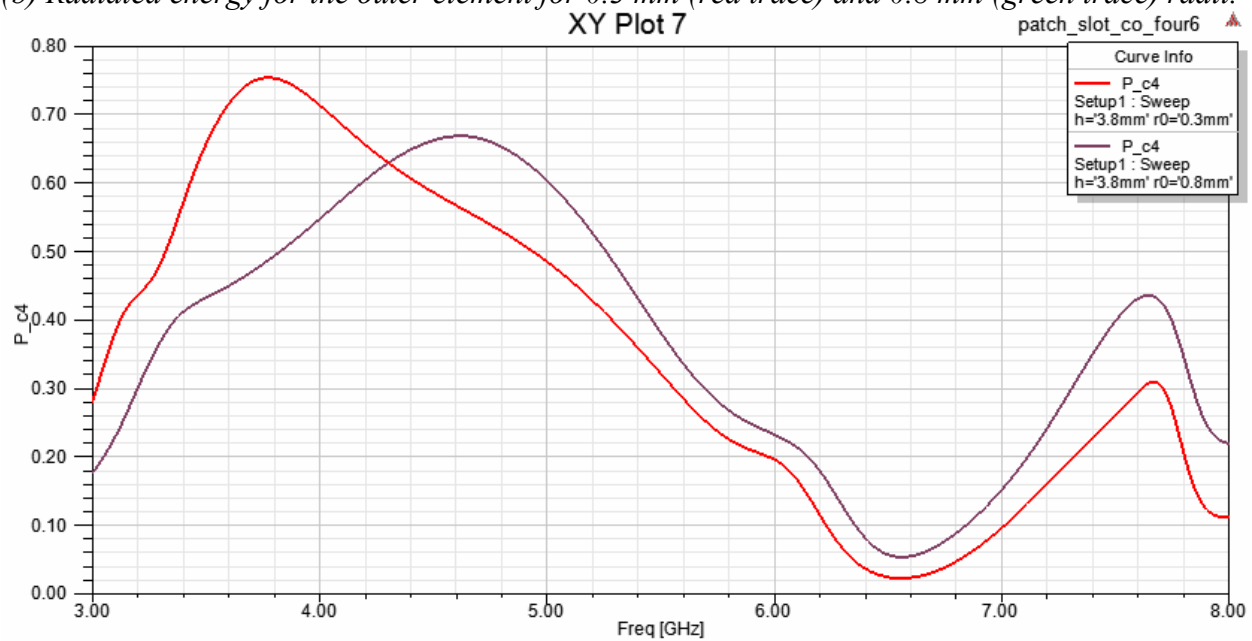
Figure 6: input impedance of the inner element for the 0.3 mm case (blue trace) and 0.8 mm case (red trace). Solid traces are the real part of the impedance. Dashed traces are the imaginary part of the impedance.



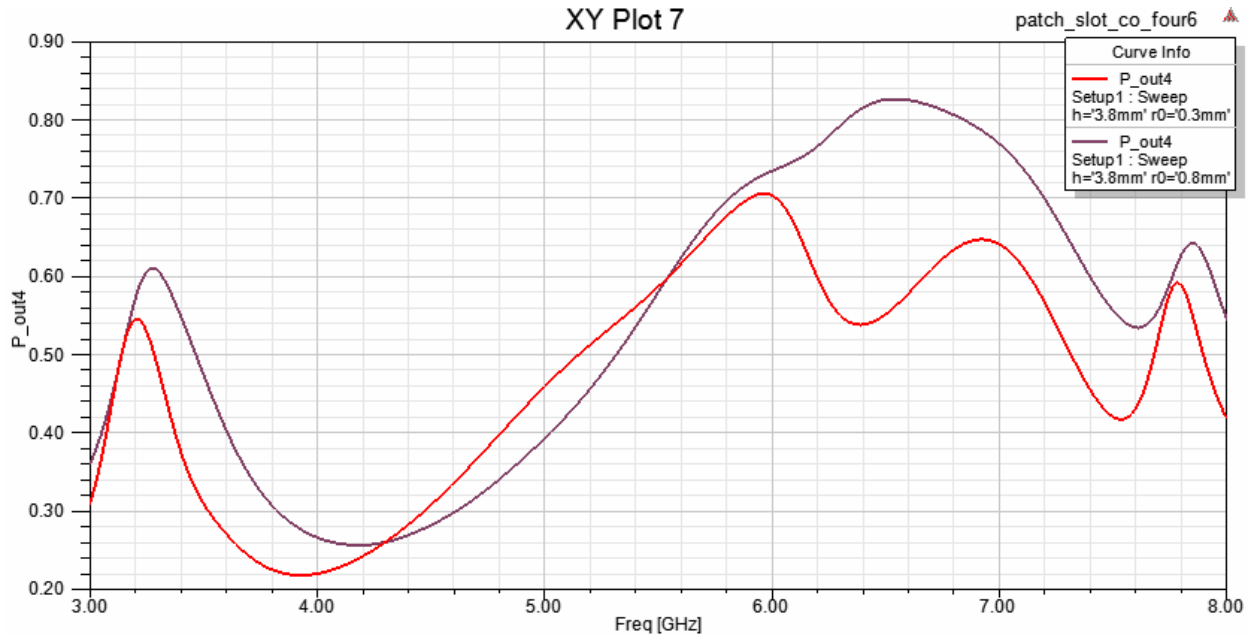
(a) Coupled energy for the outer element for 0.3 mm (red trace) and 0.8 mm (green trace) radii.



(b) Radiated energy for the outer element for 0.3 mm (red trace) and 0.8 mm (green trace) radii.



(c) Coupled energy for the inner element for 0.3 mm (red trace) and 0.8 mm (purple trace) radii.

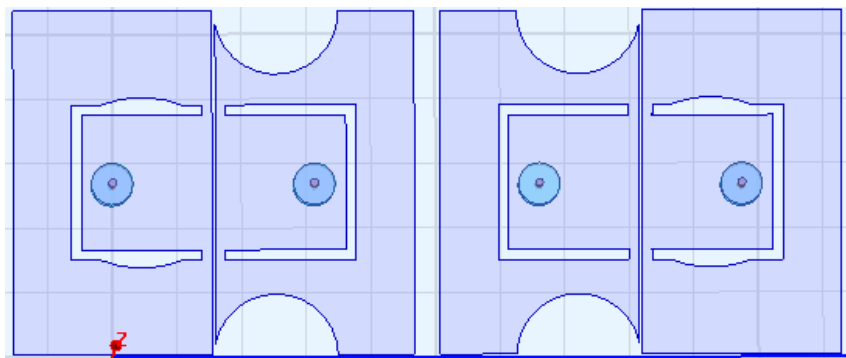


(d) Radiated energy for the inner element for 0.3 mm (red trace) and 0.8 mm (purple trace) radii. Figures 7 (a)-(d): the coupled and radiated energy for the outer element, (a) and (b), and inner element (c) and (d)

Figures 7 (a) and (c) show that peak of the coupled energy has decreased for the larger probe radius. Similarly, Figures 7 (b) and (d) show that the radiated energy increases in the higher frequency band around 7 GHz for the larger radius case. Overall Design (4) has a lower coupled peak energy and an increase in high frequency range radiation compared to Design (3) in addition to a slight increase in bandwidth symmetry.

Design (5): Introducing Arm Curvatures

To improve the bandwidth symmetry between inner and outer elements, the outer element can be manipulated to increase overall bandwidth. Previous trials of introducing a semi-circular cutout on the outer element similar to that on the inner element resulted in reduced bandwidth. So the alternative is to introduce arcs on the “arms” of the U-slots. The increase in current path near the outer edges of the arms lowers the lower frequency limit. If the curvature of the arc is parametrically varied and the bandwidth is noted, then the ideal curvature can be chosen. From Table 1 it can be seen that the outer element’s lower and upper frequency limits have increased, thus improving the bandwidth symmetry. A full analysis of the frequency behavior is presented in the next section.



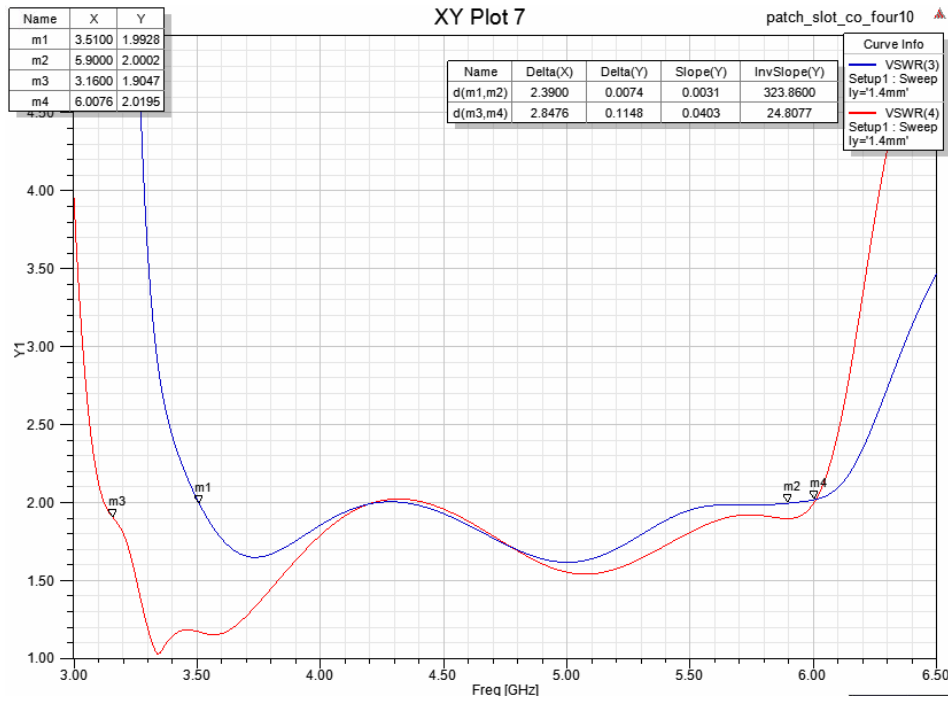


Figure 8: Geometry and bandwidth response of Design (4). Red trace is the inner element and blue trace is the outer element.

Design 6: Combination of both designs

Given the results in Designs (4) and (5), it is conducive that combining both design strategies will likely yield their combined benefits. Starting with the idealized radius of 0.8 mm, the arm curvature of the outer element is varied parametrically to achieve the widest possible bandwidth. Figures 9 and 10 show the bandwidth for design (6) with 0 mm curvature (red trace), 3 mm curvature (purple trace) and 4 mm curvature (blue trace). The zero curvature case (red trace) has a significantly higher VSWR in the low frequency range which becomes progressively lower with increasing curvature. At the meantime when the curvature is too large (4 mm case) the response overshoots the $VSWR < 2$ limit in the mid-frequency range (5.5 GHz). The optimal arm curvature was found to be at 2.2 mm. The geometry is shown in Figure 11.

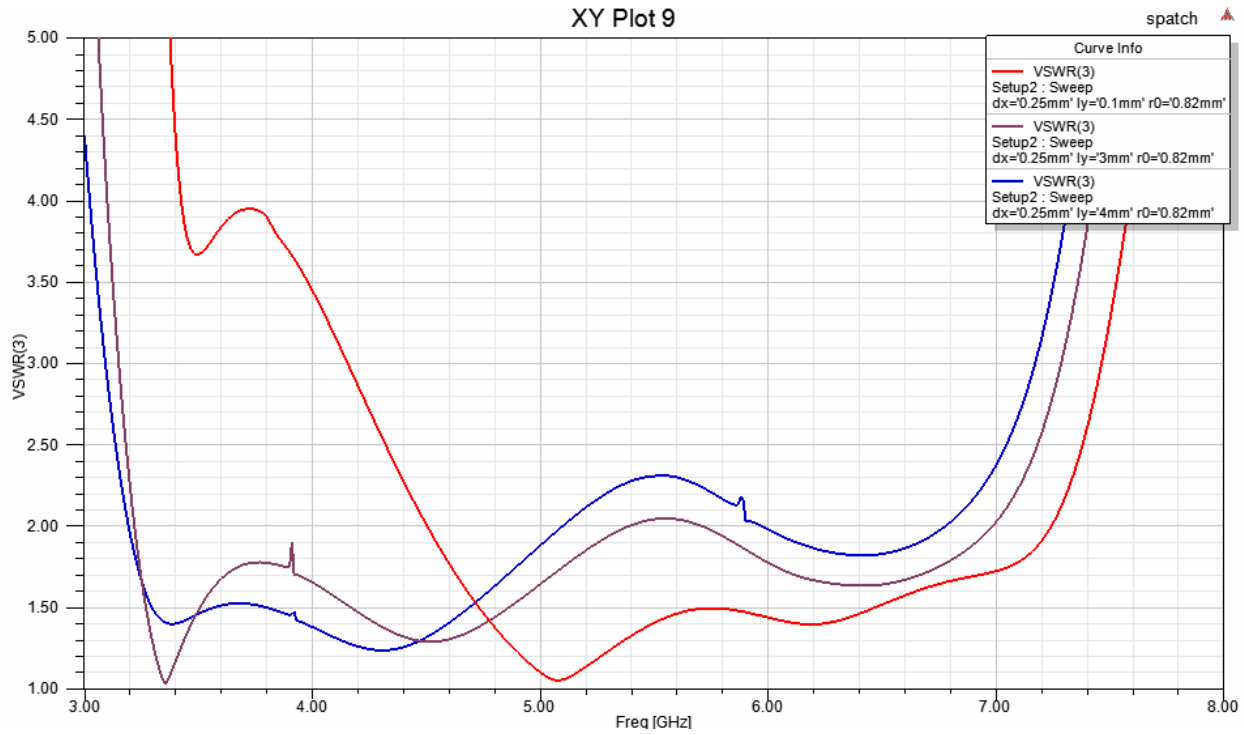


Figure 9: Bandwidth behavior of the outer element in design (6) for different arm curvatures. 0 mm curvature (red trace), 3mm curvature (purple trace) and 4 mm curvature (blue trace).

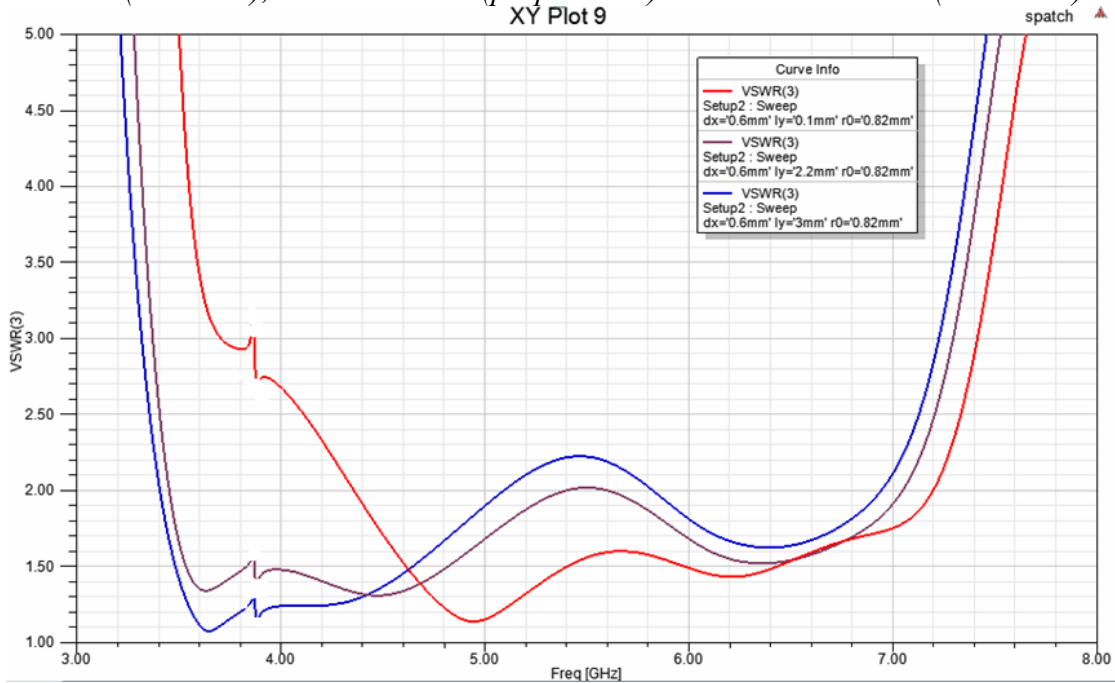


Figure 10: Bandwidth behavior of the inner element in design (6) for different arm curvatures. 0 mm curvature (red trace), 3mm curvature (purple trace) and 4 mm curvature (blue trace).

The introduction of arm curvature lowered the lower frequency limit for both the inner and outer element. In addition, the higher frequency limit set by the increase in radius was not greatly affected. The overall effect is an increase in bandwidth by 0.9 GHz and 0.8 GHz for the inner and outer elements respectively. The frequency response for the inner and outer element is shown in Figure 12. Furthermore, the bandwidth symmetry between the inner and outer element is improved again.

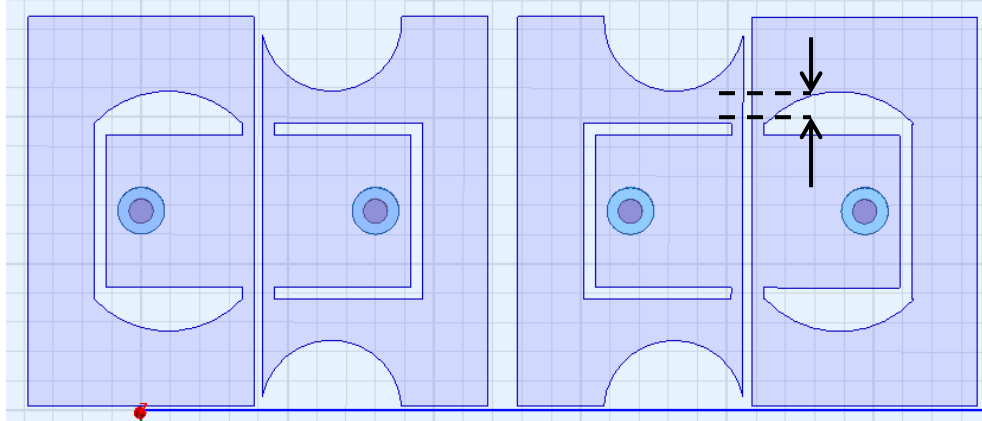


Figure 11: geometry of Design (6) for arm curvature of 2.2 mm.

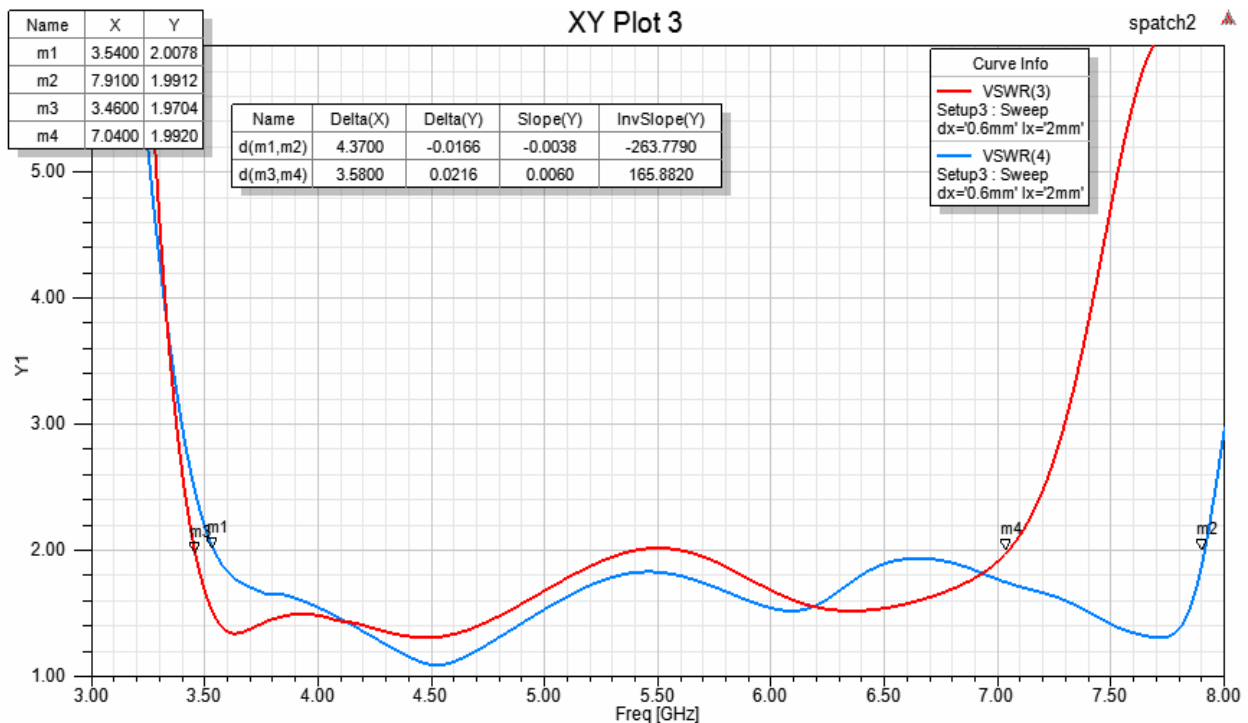


Figure 12: Bandwidth behavior for the inner (blue trace) and outer (red trace) element for the optimal case (2.2 mm curvature).

Figures 13 and 14 show the impedance response of the outer and inner elements respectively. When compared with Figures 5 and 6 of Design (4), it can be seen that both the real and imaginary parts of the impedance are more rectified particularly in the lower frequency range. This can also be verified in the Smith chart of the reflection coefficient (Figures 16 and 17). The $VSWR < 2$ frequency band is now more centered with respect to the center line (zero reactance line) as compared to the traces in figures 3 and 4. This indicates that Design (6) is more optimized and the introduction of arm curvatures does improve the overall performance.

From Figures 13 and 14, a general trend for the impedance behavior can be ascertained as follows: At the lower frequency limit, 3.5 GHz, the resistance is small while there is a large negative reactance (capacitive). The tight coupling probably has introduced high capacitances between the arms of neighboring elements, which become stronger with lower frequencies since the relative distance with respect to the wavelength becomes smaller.

Inside the bandwidth range, the impedances pass through several resonances with a periodicity of about 1.3 GHz. The ground plane contribution to the impedance is also periodic and is given by $Z_{\text{GND}} = j Z_0 / \sqrt{\epsilon_r} \tan(2\pi h/\lambda)$. However, the input impedance periodicity cannot be caused by the ground plane since the first null occurs at $\lambda/2$, far higher than the substrate thickness. It is likely caused by varying current distribution profiles on the patches, owing to their irregular geometry, that result in alternating profiles every 1.3 GHz interval. Within that interval, the current profiles set up on each patch interact in such a way to generate a distinctive equivalent RLC circuit. It rapidly transitions into a different RLC circuit, as a new current profile dominates and the effective geometry of the array becomes rescaled with increasing frequency. These cycles continue until a limit is reached, based on the array size, which can no longer support enough coupling between the elements to counteract the inductance due to the ground plane. Thus at the higher frequency limit the reactance is positive (inductive) as shown in figure 14 around 7.8 GHz.

Based on the number of resonance points in Figures 13 and 14, it can be surmised that the equivalent circuit is not a simple parallel RLC system as this will result in a single resonance point for the imaginary impedance (second order circuit). The required circuit is at least seventh order. A similar trend in the impedance response is also reported by Tzanidis [1] in their thesis where wideband array is designed based on a large square array of tightly coupled spirals. Figure 15 shows the impedance response for the spiral element array compared to two traditional wideband designs: the current sheet array and tightly coupled bow-tie antennas. Only the spiral design exhibits the highly oscillatory behavior in the impedance. Tzanidis reports that the ripples in the spiral's impedance depends on the number of turns within a given unit cell size indicating a dependence on how currents are set up on non-uniform geometries. All three designs exhibit wider bandwidth response since they are not backed by a ground plane.

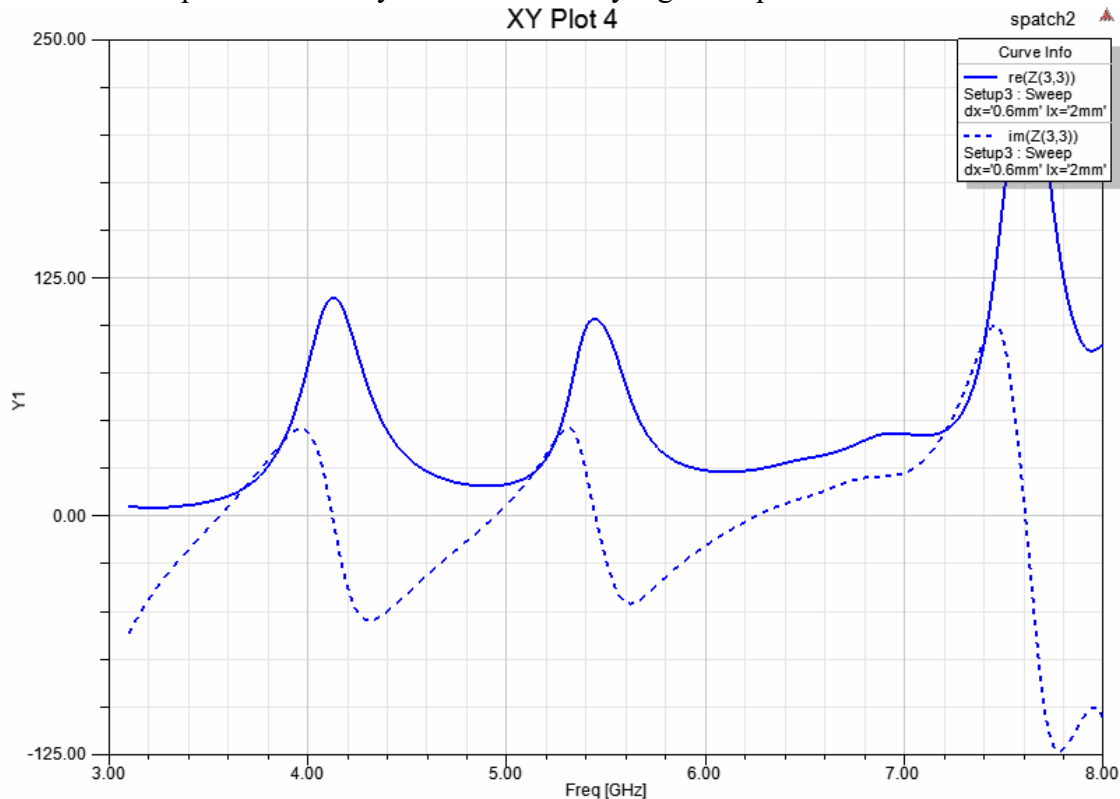


Figure 13: Real (solid trace) and imaginary (dashed trace) parts of the impedance for the outer element.

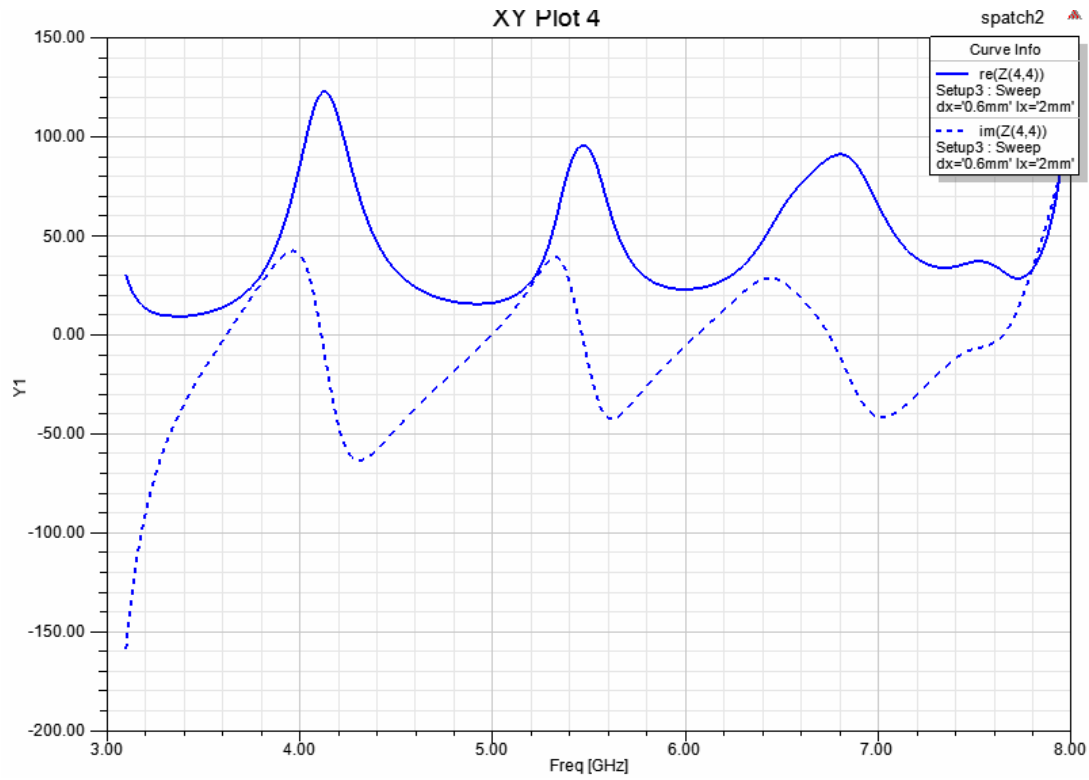
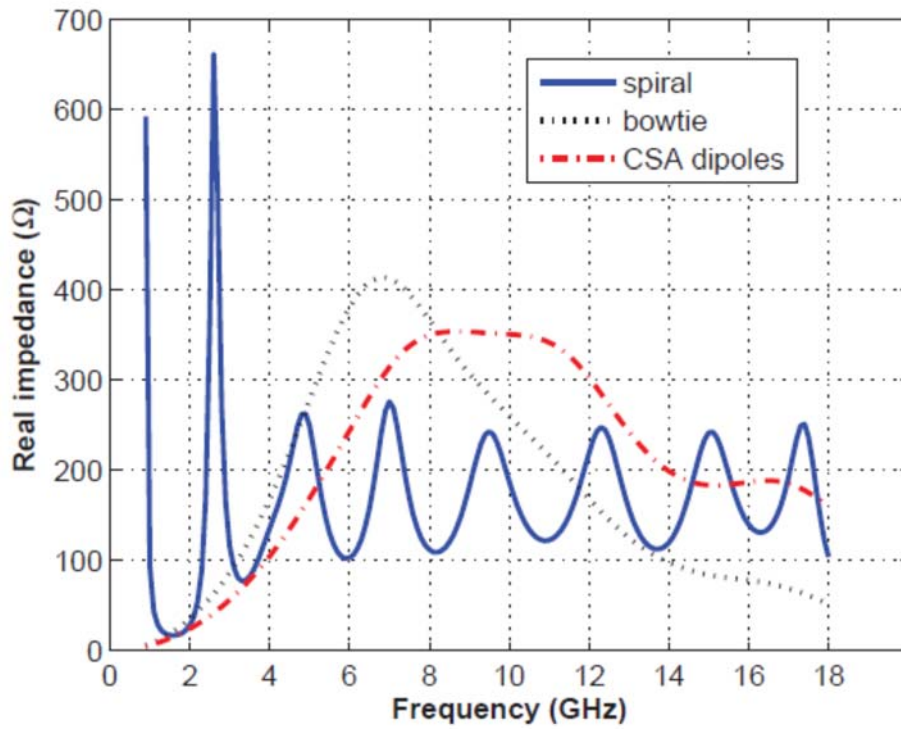


Figure 14: Real (solid trace) and imaginary (dashed trace) parts of the impedance for the inner element.



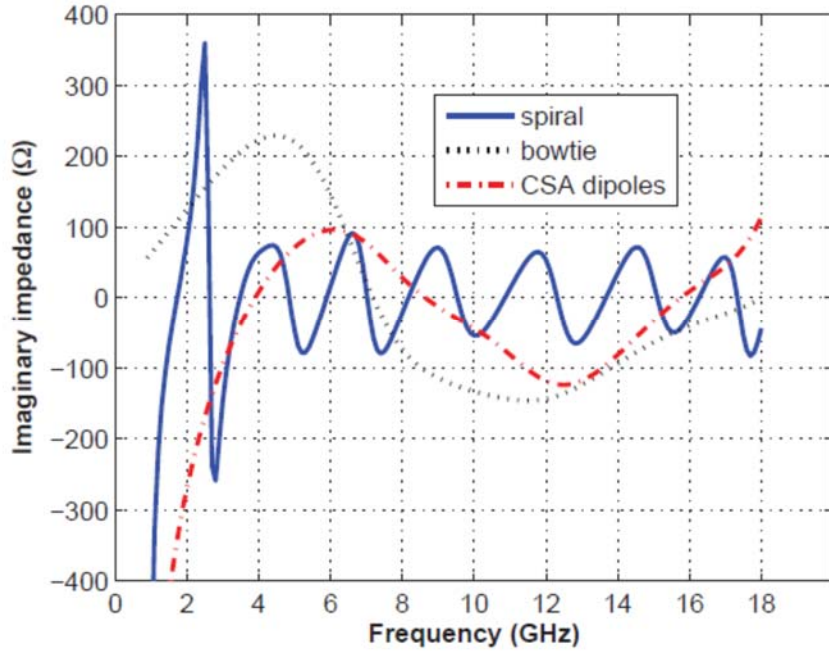


Figure 15: Impedance response of spiral element array compared to bowtie and current sheet array. It can be concluded that small linear arrays require asymmetrical elements to compensate for the asymmetry experienced by the edge elements and simply arraying identical elements worsens the performance of the overall array and does not utilize its full bandwidth potential.

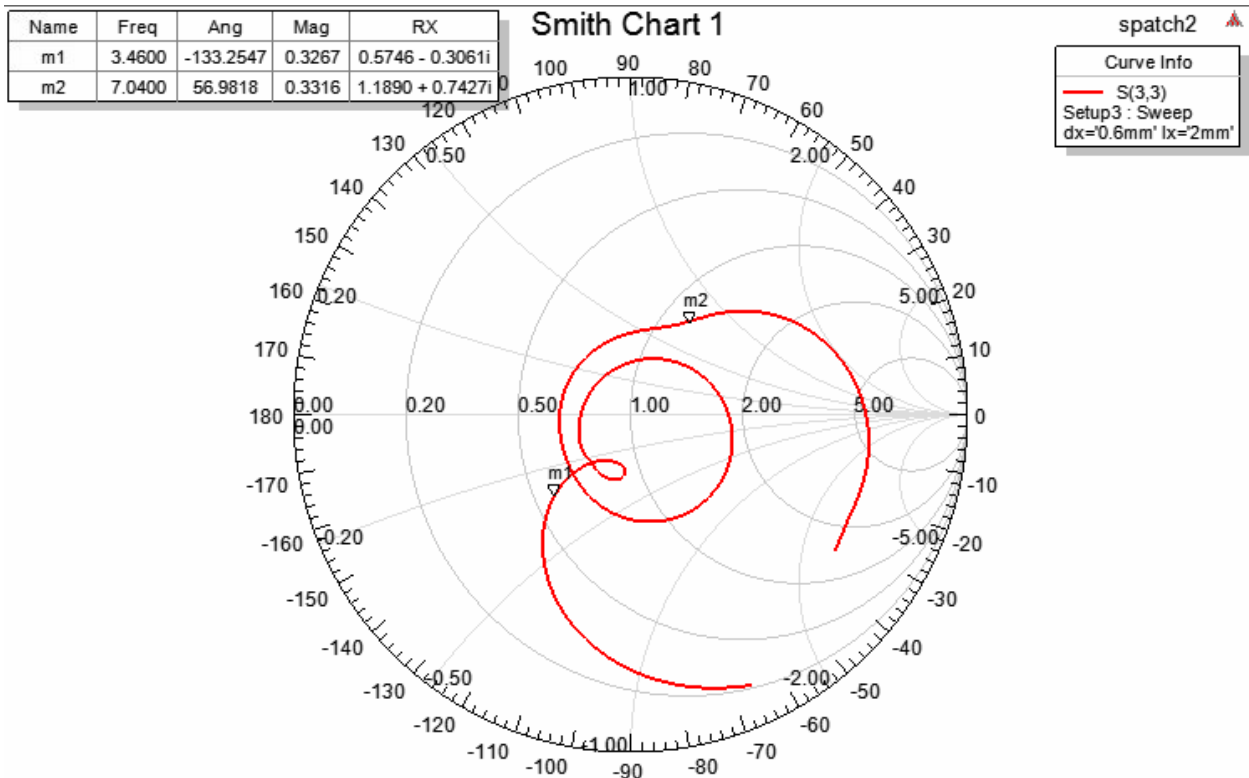


Figure 16: Smith chart of the reflection coefficient of the outer element.

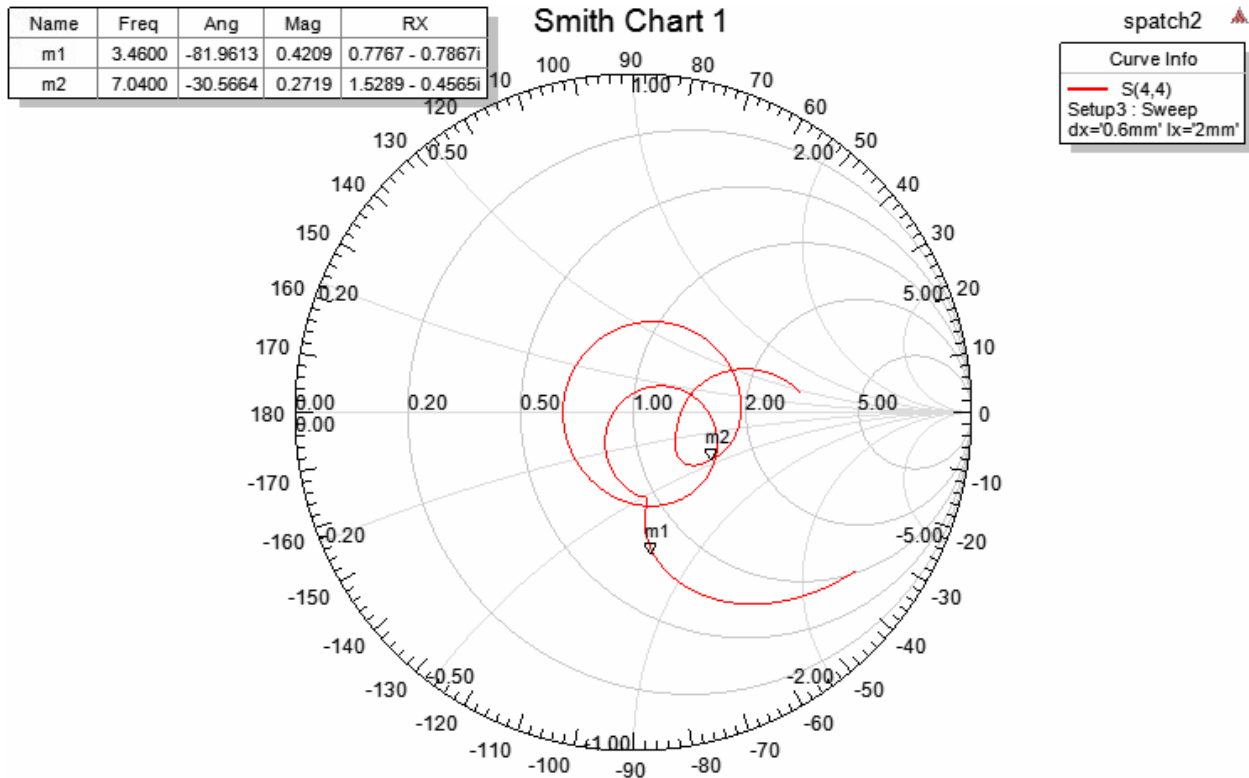


Figure 17: Smith chart of the reflection coefficient of the inner element.

Future Work

This project has demonstrated that careful and theory-based design of small, wideband arrays is possible. The extensions of this project into the future can include the creation of an array-based model that captures the characteristics of the coupling and bandwidth properties necessary for each element to deliver on the total array specification. As part of this, a generalized coupling model for individual elements such that the properties (though not the geometries) of each element can be specified to deliver desired performance for any particular set of volumetric and material constraints. Additionally, the ability of the array and individual element performance to be maintained throughout beam scan should certainly be investigated.

References:

[1] Tzanidis, I., “Ultrawideband Low-Profile Arrays of Tightly Coupled Antenna Elements: Excitation, Termination and Feeding Methods,” The Ohio State University, 2011.